Asian Research Journal of Mathematics

6(4): 1-23, 2017; Article no.ARJOM.36303
ISSN: 2456-477X

Thermo-diffusion and Diffusion-thermo Effects on MHD Micropolar Fluid Flow Over a Linearly Stretching Sheet, Through a Non-Darcy Porous Medium

Bhim Sen Kala[1*], Madan Singh Rawat[2], M. S. Bist[3] and Nimisha Rawat[2]

[1]Department of Mathematics, K L University, Guntur, Andhra Pradesh, India.
[2]Department of Mathematics, H. N. B. Garhwal University, Srinagar Garhwal, Uttarakhand, India.
[3]Department of Mathematics, G. B. P. Engineering College, Pauri Garhwal, Uttarakhand, India.

Authors' contributions

This work was carried out in collaboration between all authors. Author BSK designed the study, performed the analysis, wrote the protocol, and wrote the first draft of the manuscript. Author MSR managed the analyses of the study. Authors MSB and NR managed the literature searches. All authors read and approved the final manuscript.

Article Information

DOI: 10.9734/ARJOM/2017/36303
Editor(s):
(1) Jitender Singh, Guru Nanak Dev University, Punjab, India.
Reviewers:
(1) Mohammad Yaghoub Abdollahzadeh Jamalabadi Dongguk, Dongguk University, Korea.
(2) Sanjib Kumar Datta, University of Kalyani, India.
(3) Sherin Zafar, India.
Complete Peer review History: http://www.sciencedomain.org/review-history/21217

Original Research Article

Received: 22nd August 2017
Accepted: 25th September 2017
Published: 3rd October 2017

Abstract

In this paper, the thermo-diffusion and Diffusion-thermo effects on MHD micropolar fluid flow over a linearly stretching sheet, through a non -Darcy porous medium, where stretching velocity of the sheet varies linearly with distance from the origin, and, temperature and concentration vary non linearly in the boundary layer region, is discussed. By suitable similarity transformations, the governing boundary layer equations are transformed to ordinary differential equations and to solve these equations the method applied is numerical computation with bvp4c, a MATLAB program. The effects of Magnetic Parameter, Soret number and Dufour number on velocity profiles, microrotation profile, heat transfer, and concentration, Skin- Frictions, local Nusselt Number and local Sherwood Number are computed, discussed and analysed numerically and presented through tables and graphs.

Keywords: MHD Flow; magnetic parameter; Dufour number; soret number.

**Corresponding author: E-mail: bhimskala@gmail.com;*

1 Introduction

Erigen [1] introduced the fluid model which exhibit some microscopic effects arising from the local structure and micromotion of the fluid elements; they can sustain couple stresses and include Newtonian fluid as a special case. The micropolar fluid model represents fluid consisting of rigid, randomly oriented (or spherical) particles suspended in a viscous medium; here deformation of the particles is ignored. It is shown that micropolar fluids accurately simulate the flow characteristics of polymeric additives, geomorphological sediments, colloidal suspensions, haematological suspensions, liquid crystals, etc.

Sakiadis [2] first studied the flow field due to moving surface with constant velocityin a quiescent fluid. Crane [3] worked on the dynamics of the boundary layer flow over a stretching surface. Nield and Bejan [4] had discussed the analysis and application of convective transport in a porous media.

Lukaszewicz [5] had presented the mathematical theory of equations of micropolar fluids and their applications in the theory of lubrication and in the theory of porous media.

Srinivasacharya et al. [6] have analysed the flow of fluid, heat and mass transfer with free convection over a vertical plate with variable temperature and concentration in a doubly stratified micropolar fluid, in the presence of magnetic field normal to the plates.

Ramachandran et al. [7] studied the influence of Prandtl number, the ratio of momentum to heat diffusivity in coquette flowsat high Mach numbers. Khalid et al. [8] investigated the unsteady flow of a micropolar fluid with free convection over a vertical plate oscillating in its own plane.

Nadeem et al. [9] analysed the optimal and numerical solutions for the MHD micropolar nanofluid flow and heat transfer between rotating horizontal parallel plates.

Das [10] studied the effects of radiation, chemical reaction, temperature dependent fluid properties, and partial slip on the MHD micropolar fluid flow, heat and mass transfer over an inclined permeable plate with constant heat flux and non-uniform heat source /sink.

Adhikari et al. [11] analysed the effect of radiation on the MHD micro polar fluid flow and heat transferover a stretching or shrinking vertical sheet under the suction or blowing.

Matin et al. [12] investigated the effects of viscous dissipation and variable magnetic field over MHD nano fluid flow with mixed convection, and heat transfer over a nonlinear stretching sheet.

Chaudhary et al. [13] studied the effect of chemical reaction on the unsteady MHD micro polar fluid flow, heat and mass transfer past a semi infinite vertical plate in a slip-flow regime in a porous medium. Ali, et al. [14] presented the numerical study of unsteady MHD water based nano fluid flow, and heat transfer between two orthogonally moving porous coaxial disks with suction .

Mohyud-Din et al. [15] studied the optimal and numerical solutions of MHD micropolar nano fluid flow through a porous channel with radiation effect. El-Dabe et al. [16] studied MHD micropolar fluid flow with heat and mass transfer towards at stagnation point on a vertical plate. Maripala et al. [17] had studied the effects of variable thermal conductivity and radiation on the MHD micro polar fluid flow, heat and mass transfer over a continuously stretching surface with varying temperature and in the presence of magnetic field.

Chamkha et al. [18] investigated the effects of Joule-heating, chemical reaction and thermal radiation on unsteady MHD micropolar fluid flow with natural convection, heat and mass transfer from a heated vertical porous plate.

Sandeep et al. [19] analysed the unsteady boundary layer flow of thermophoretic MHD nanofluid past a stretching sheet with space and time dependent internal heat source /sink, in a porous medium. Khedr, et al. [20] investigated the steady laminar MHD micro polar fluid flow and heat transfer past a semi infinite vertical and permeable surface in the presence of temperature dependent heat generation or absorption, magnetic field, and thermal radiation.

Sandeep et al. [21] analysed the influence of non uniform source /sink and chemical reaction on unsteady MHD micropolar fluid flow with mixed convection, heat and mass transfer, over a stretching /shrinking sheet in the presence of viscous dissipation and suction/injection.

Satya Narayana et at. [22] studied the effects of Hall current and radiation absorption on MHD fluid flow with free convection, heat and mass transfer of a micropolar fluid in a rotating frame of reference. Kelson, et al. [23] studied the effects of surface condition like uniform suction or blowing through the surface, over the micropolar fluid flow due to the stretching surface.

Pal D et al. [24], analyzed the effects of viscous-Ohmic dissipation and variable thermal conductivity on steady two-dimensional hydromagnetic flow, heat and mass transfer of a micropolar fluid over a stretching sheet embedded in a non-Darcian porous medium with non-uniform heat source/sink and thermal radiation.

In the above work Dufour and Soret effects on MHD micropolar fluid flow over a non-Darcy porous medium is not studied.

The presented work studies Dufour and Soret effects on MHD micropolar fluid flow over a non-Darcy porous medium.

2 Mathematical Formulation of the Problem

Assumptions: Micropolar fluid is incompressible and electrically conducting. Fluid flow is two dimensional over the porous surface coinciding with the plane $y = 0$ and the flow region is $y > 0$. The *x*-axis is taken in the direction along motion of the sheet and the *y*-axis is taken perpendicular to it. The flow is generated by the action of two equal and opposite forces along the *x*-axis and the sheet is stretched in such a way that the velocity at any instant is proportional to the distance from the origin ($x = 0$).An external magnetic field of strength $B = (0, B_0, 0)$ is applied normal to the surface. The hole size of the porous surface is constant. The non-Darcian inertia effect is considered in the model. The thermal conductivity of the fluid is assumed to be functions of temperature. There is a first order chemical reaction between the diffusing species and the fluid. The effect of thermal radiation, thermo-diffusion and diffusion-thermo are considered. Reynolds number is assumed to be small. The pressure gradient, body forces, the Hall currents, frictional heating due to viscous dissipation and Ohmic heating due to application of magnetic field are negligible and hence not considered in the present model.

The temperature and concentration of the plate surface is always greater than their free stream values. The flow configuration and the coordinate system are shown in Fig. 1.

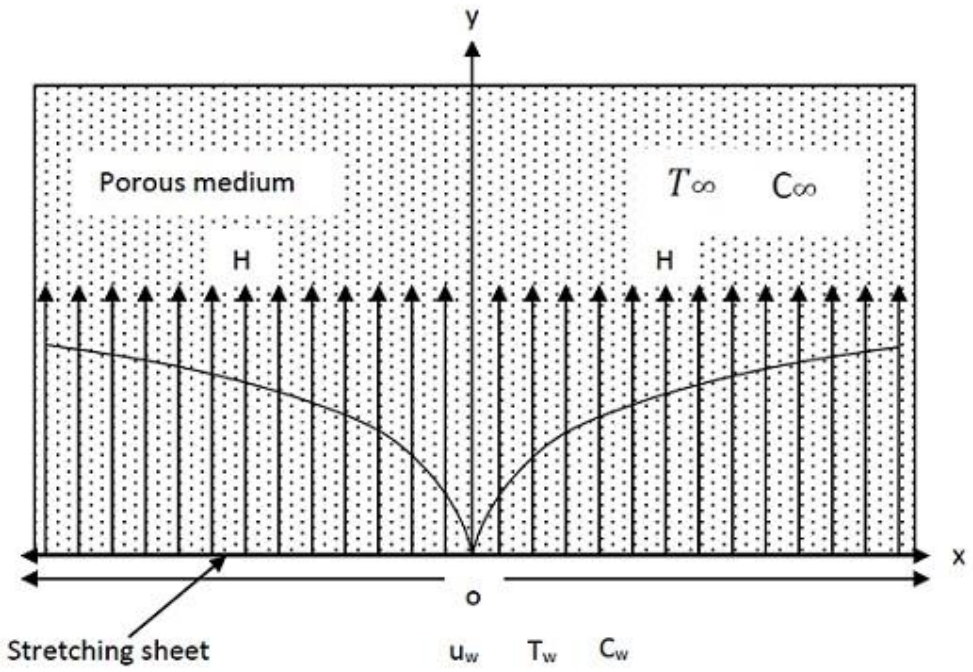

Fig. 1. Physical flow model over stretching surface

Under the foregoing assumptions and using the Boussinesq approximation, the governing equations describing the physical model can be written as follows:

The continuity equation:

$$\frac{\partial u}{\partial x}+\frac{\partial v}{\partial y}=0 \quad , \tag{1}$$

The equation of momentum:

$$u\frac{\partial u}{\partial x}+v\frac{\partial u}{\partial y}=\left(\frac{\mu+\kappa_V}{\rho}\right)\frac{\partial^2 u}{\partial y^2}+\left(\frac{\kappa_V}{\rho}\right)\frac{\partial N}{\partial y}$$
$$+g\beta_T(T-T_\infty)+g\beta_C(C-C_\infty)-\frac{\sigma B_0^2}{\rho}u-\frac{\upsilon}{k_p}u-\frac{C_E}{\sqrt{k_p}}u^2 \tag{2}$$

The equation of angular momentum:

$$u\frac{\partial N}{\partial x}+v\frac{\partial N}{\partial y}=\left(\frac{\gamma}{\rho\, j}\right)\frac{\partial^2 N}{\partial y^2}-\left(\frac{\kappa_V}{\rho\, j}\right)\left(2N+\frac{\partial u}{\partial y}\right) \tag{3}$$

The equation of energy:

$$u\frac{\partial T}{\partial x}+v\frac{\partial T}{\partial y}=\frac{1}{\rho C_p}\frac{\partial}{\partial y}\left(k\frac{\partial T}{\partial y}\right)-\frac{1}{\rho C_p}\frac{\partial q_r}{\partial y}+\left(\frac{D_M K_T}{C_S C_P}\right)\frac{\partial^2 C}{\partial y^2} \tag{4}$$

The equation of mass concentration:

$$u\frac{\partial C}{\partial x}+v\frac{\partial C}{\partial y}=D_M\frac{\partial^2 C}{\partial y^2}-k_c\left(C-C_\infty\right)+\left(\frac{D_M K_T}{T_M}\right)\frac{\partial^2 T}{\partial y^2} \tag{5}$$

where u and v are velocity components along x and y axes, respectively; κ_v is micro-rotation viscosity or the vortex viscosity; j is the micro-inertia density; μ is the dynamic viscosity; υ is the kinematic viscosity. N is the microrotation components normal to the $x-y$ plane; γ is the spin gradient viscosity ; σ is the electrical conductivity of the fluid and is assumed to be constant; k_p is permeability of the porous medium; C_E is the form of drag coefficient which is independent of viscosity and other properties of the fluid but depends on the geometry of the medium, β_T is the coefficient of thermal expansion, β_C is the coefficient of concentration expansion, T is the temperature of the fluid , T_W is the temperature of the fluid at the surface, T_∞ is the temperature of the fluid outside the boundary layer, k is the thermal conductivity of the fluid, C_P is the specific heat at constant pressure P; D_M is the chemical molecular diffusivity; k_c is chemical reaction constant. ρ is the density of the fluid; g is the acceleration due to gravity. The applied magnetic field B_0 is a constant. j, μ and γ are non negative.

Boundary conditions:

$$\begin{aligned}
&At\ y=0: u=u_w=bx,\ v=0,\ \ N=-m\frac{\partial u}{\partial y},\\
&T=T_w=T_\infty+A_0\left(\frac{x}{l}\right)^2,\ C=C_w=C_\infty+A_1\left(\frac{x}{l}\right)^2,\\
&As\ \ y\to\infty: u\to 0,\ N\to 0, T\to T_\infty,, C\to C_\infty.
\end{aligned} \tag{6}$$

The thermal conductivity k is assumed to vary linearly with temperature and it is of the form $k=k_\infty\left(1+\varepsilon\theta(\eta)\right)$ where $\theta(\eta)=\left(T-T_\infty\right)/\left(T_W-T_\infty\right)$ and $\varepsilon=\left(k_w-k_\infty\right)/k_\infty$ which depends on the nature of the fluid and is a small parameter. k_w is thermal conductivity at the surface, k_∞ is thermal conductivity of the fluid far away from the surface. Here, ε is thermal coefficient (constant); $\varepsilon>0$ for air and liquids such as water, while $\varepsilon<0$ for fluids such as lubrication oils.

Following Rosseland approximation the radiative heat flux q_r is modelled as $q_r=-\left(4\sigma^*/3k^*\right)\left(\partial T^4/\partial y\right)$ where σ^* is the Stefan- Boltzmann constant and k^* is the mean

absorption coefficient. It is assumed that the temperature difference within the flow is such that the term T^4 may be expressed as a linear function of temperature. Hence expanding T^4 by Taylor's series about T_∞ gives $T^4 = T_\infty^4 + 4T_\infty^3(T-T_\infty) + 6T_\infty^2(T-T_\infty)^2 + \ldots\ \ldots$;
and then neglecting higher order terms beyond the first degree in $(T-T_\infty)$ we get $T^4 = 4T_\infty^3 T - 3T_\infty^4$.

And so

$$q_r = -\left(4\sigma^*/3k^*\right)\left(\partial\left(4T_\infty^3 T - 3T_\infty^4\right)/\partial y\right) = -\left(16\sigma^*/3k^*\right)T_\infty^3\left(\partial T/\partial y\right) \tag{7}$$

$$\frac{\partial q_r}{\partial y} = -\frac{16\sigma^* T_\infty^3}{3k^*}\frac{\partial^2 T}{\partial y^2}. \tag{8}$$

Using this in equation (4) we get

$$u\frac{\partial T}{\partial x} + v\frac{\partial T}{\partial y} = \frac{1}{\rho C_p}\frac{\partial}{\partial y}\left(k\frac{\partial T}{\partial y}\right) - \frac{1}{\rho C_p}\frac{\partial\left(-\left(16\sigma^*/3k^*\right)T_\infty^3\left(\partial T/\partial y\right)\right)}{\partial y} + \left(\frac{D_M K_T}{C_S C_P}\right)\frac{\partial^2 C}{\partial y^2} \tag{9}$$

Or

$$u\frac{\partial T}{\partial x} + v\frac{\partial T}{\partial y} = \frac{1}{\rho C_p}\frac{\partial}{\partial y}\left(\left(k + \frac{16\sigma^* T_\infty^3}{3k^*}\right)\frac{\partial T}{\partial y}\right) + \left(\frac{D_M K_T}{C_S C_P}\right)\frac{\partial^2 C}{\partial y^2}. \tag{10}$$

To investigate the effect of different surface conditions, we choose a linear relationship between microrotation variable N and the surface stress $\frac{\partial u}{\partial y}$ in the boundary conditions (6); m is the proportionality constant. Here, the microrotation parameter m ranges between 0 and 1 $(0 \le m \le 1)$. When $m = 0$, we have $N = 0$, which is a generalisation of the no-slip condition, that is, the particle density is sufficiently large so that microelements close to the surface are not able to translate or rotate. The case $m = 0.5$ represents the vanishing of anti-symmetric part of the stress tensor and represents weak concentration of the microelements. For this case, in a fine particle suspension, the particle spin is equal to the fluid velocity at the surface. The value of $m = 1$ is used for the modelling of turbulent flow inside the boundary layers of microrotation.

Dimensional Analysis: We consider following dimensionless variable

$$\eta = y\left(\frac{b}{\upsilon}\right)^{\frac{1}{2}},\ N = b\,x\left(\frac{b}{\upsilon}\right)^{\frac{1}{2}}h(\eta),\ u = b\,x\,f'(\eta),$$
$$v = -(b\upsilon)^{\frac{1}{2}}f(\eta),\ \theta(\eta) = \frac{(T-T_\infty)}{(T_w-T_\infty)},\ \phi(\eta) = \frac{(C-C_\infty)}{(C_w-C_\infty)}, \tag{11}$$

η is the similarity variable.

Introducing the variables in the equations (2), (3), (4) and (5), we get the following dimensionless forms of the equations:

$$(1+K_{mp})f''' + f\,f'' - f'^2 + K_{mp}\,h' + Gr_T\,\theta + Gr_C\,\phi - (M+(1/Da))f' - Fs\,(f')^2 = 0 \quad , \tag{12}$$

$$\left(1+K_{mp}/2\right)h'' + (h'f - hf') - K_{mp}(2h + f'') = 0 \quad , \tag{13}$$

$$\frac{\left(1+\varepsilon\theta+R\right)}{\Pr}\theta'' + f\,\theta' - 2f'\theta + Du\;\phi'' + \frac{1}{\Pr}\varepsilon\theta'^2 = 0 \quad , \tag{14}$$

$$\frac{1}{Sc}\phi'' + f\,\phi' - 2f'\phi - K_c\phi + Sr\,\theta'' = 0 \quad . \tag{15}$$

Where

$$\begin{aligned}
&j = \frac{\upsilon x}{u_w},\ M = \frac{\sigma B_0^2}{\rho b},\ Gr_T = \frac{g\,\beta_T\,(T_W - T_\infty)}{b^2},\\
&Gr_c = \frac{g\,\beta_C\,(C_W - C_\infty)}{b^2},\ K_{mp} = \frac{k_v}{\mu},\\
&\gamma = \left(\mu + \frac{k_v}{2}\right)j = \mu\left(1 + \frac{k_v}{2\mu}\right)j = \mu\left(1 + \frac{K_{mp}}{2}\right)j,\\
&\frac{\gamma}{j\rho\upsilon} = 1 + \frac{K_{mp}}{2},\ \frac{k_v}{j\rho b} = \frac{b k_v}{\upsilon\rho b} = \frac{k_v}{\mu} = K_{mp},\\
&j = \frac{\upsilon x}{u_w} = \frac{\upsilon}{b},\ Da = \frac{b k_p}{\upsilon},\ Fs = \frac{C_E\,x}{\sqrt{k_p}}, K_c = \frac{k_c}{b},\\
&\Pr = \frac{\upsilon}{\alpha} = \frac{\upsilon\rho C_p}{k},\ R = \frac{16\sigma^* T_\infty^3}{3k^* k},\ Sc = \frac{\upsilon}{D_M},\\
&Du = \frac{D_M\ K_T\ (C_W - C_\infty)}{\upsilon C_S\,C_P\,(T_W - T_\infty)},\ Sr = \frac{D_M\ K_T\ (T_W - T_\infty)}{\upsilon T_M\,(C_W - C_\infty)}.
\end{aligned} \tag{16}$$

Here the names of the symbols used above are as follows: The micro-inertia per unit mass (reference length) j , Magnetic parameter (Hartmann number) M , Thermal Grashof number Gr_T , Concentration Grashof number Gr_c , The micropolar or material parameter K_{mp} , The spin gradient viscosity γ , The Darcy porosity parameter Da , The Forchheimer parameter Fs , The Prandtl number, $\Pr$,

The radiation Parameter R , Dufour (thermo-diffusion)parameter Du , Schmidth number $Sc = \frac{\upsilon}{D_M}$, Soret (diffusion-thermo)parameter Sr , Chemical reaction parameter K_c .

And corresponding boundary conditions as follows:

$$\begin{aligned} &f(0) = 0, \quad f'(0) = 1, \quad h(0) = -m\ f''(0) \quad \theta(0) = 1 \quad ,\phi(0) = 1; \\ &f'(\infty) = 0 \quad h(\infty) = 0 \quad ,\theta(\infty) = 0,\ \phi(\infty) = 0. \end{aligned} \tag{17}$$

The quantities of physical interest are the Skin friction coefficient (rate of shear stress), the couple stress coefficient at the surface, the local Nusselt number (rate of heat transfer) and the local Sherwood number (rate of mass transfer).

The Skin friction coefficient is defined as

$$C_f = \frac{\tau_W}{\frac{1}{2}\rho u_w^2} = -2\left(\mathrm{Re}_x\right)^{-\frac{1}{2}} f''(0) \quad , \tag{18}$$

The couple stress coefficient at the surface is defined as follows:

$$C_r = \frac{\frac{\gamma}{k_v}\left(\frac{\partial N}{\partial y}\right)_{y=0}}{\gamma\ U_0^3\ (2 k_v \upsilon^2)} = \left(\mathrm{Re}_x\right)^{-1} h'(0) \quad . \tag{19}$$

The rate of heat transfer in terms of the dimensionless local Nusselt number is defined as follows:

$$Nu_x = \frac{x\, q_W}{k\,(T_W - T_\infty)} = -2\left(\mathrm{Re}_x\right)^{-\frac{1}{2}} \theta'(0) \quad , \tag{20}$$

The rate of mass transfer in terms of the dimensionless local Sherwood number is defined as follows:

$$Sh_x = \frac{x\, J_W}{D_M\ (C_W - C_\infty)} = -2\left(\mathrm{Re}_x\right)^{-\frac{1}{2}} \phi'(0) \quad . \tag{21}$$

The surface shear stress is defined as follows:

$$\tau_W = \left(\mu + k_v\right)\left(\frac{\partial u}{\partial y}\right)_{y=0} + \left(k_v\ N\right)_{y=0} \quad . \tag{22}$$

The heat flux is defined as follows:

$$q_W = -k\left(\frac{\partial T}{\partial y}\right)_{y=0}. \tag{23}$$

The Mass flux is defined as follows:

$$J_W = -D_M\left(\frac{\partial C}{\partial y}\right)_{y=0}. \tag{24}$$

The local Reynold number is defined as follows: $\mathrm{Re}_x = \frac{u_w\, x}{\upsilon}$.

3 Method of Numerical Solution

The numerical solutions are obtained using the above equations for some values of the governing parameters, namely, the Magnetic Parameter (M), the Dufour number(Du), the Soret number (Sr), thermal coefficient parameter (ε) and slip parameter (m). Effects of M, Sr, and Du, on the steady boundary layers in fluid flow region are discussed in detail. The numerical computation is done using the MATLAB in-built Numerical Solver bvp4c. In the computation we have taken $\eta_\infty = 8.0$ and axis according to the clear figure-visibility. Below we have used 'e' to represent 'ε'.

4 Results and Discussion

The non-dimensional linear velocity $f'(\eta)$, angular velocity $h(\eta)$, temperature $\theta(\eta)$, and concentration $\phi(\eta)$ for various values of different parameters are shown in Figs. 2 to 18.

To ensure the numerical accuracy, the values of $-\theta'(0)$ by present method are compared with the results of Ishak *et al*. (2008), Chen (1998), Grubka and Bobba(1985) and D. Pal and S. Chatterjee(2015) in Table 1 for various values of Pr and Da=inf, Fs=0.0, Gr_T=0.0, Gr_c=0.0, K_{mp}=0.0, Sc=0.0, m=0.0, M=0.0, Pr=1.0, R=0.0, e=0.00, Du=0.00, Sr=0.00, Kc=0.0 and f''(0)=0 and those are found in excellent agreement with the present values. Thus, we are very much confident that the present results are accurate.

Table 1. Comparison of the local Nusselt number $-\theta'(0)$ with Ishak et al. (2008), Chen (1998), Grubka and Bobba (1985)and D. Pal and S. Chatterjee(2015), and present results for various values of Pr and Da=inf, Fs=0.0, Gr_T=0.0, Gr_c=0.0, K_{mp}=0.0, Sc=0.0, m=0.0, M=0.0, Pr=1.0, R=0.0, e=0.0, Du=0.0, Sr=0.0, K_c=0.0, f''(0)=0.0

Pr	$\theta'(0)$				$\theta'(0)$
	Ishak et al. (2008)	Chen (1998)	Grubka and Bobba(1985)	D. Pal and S. Chatterjee(2015)	Present Results
1	1.3333	1.33334	1.3333	1.333333	1.333346
3	2.5097	2.50997	2.5097	2.509725	2.509682
10	4.7969	4.79686	4.7969	4.796873	4.796226

The effects of the magnetic parameter on the translational velocity, microrotation , temperature , and concentration distribution are presented in Figs. 2–5.

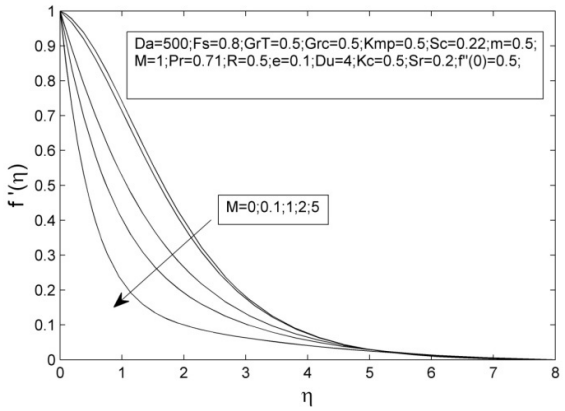

Fig. 2. Variation in the value of fluid velocity with M , the Magnetic parameter

Fig. 2 shows the velocity field decreases asymptotically with the increase in magnetic parameter M. The fluid velocity decreases sharply when $0 < \eta < 2.5$ and when $2.5 < \eta$, it decreases slowly and almost becomes constant. This shows velocity boundary layer thickness decreases with the increase in the magnetic parameter.

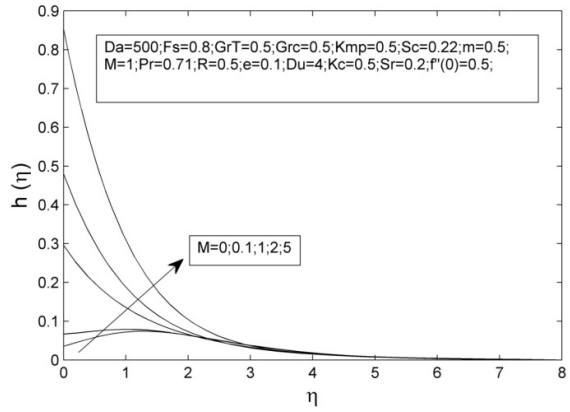

Fig. 3. Variation in the value of angular velocity with M , the Magnetic parameter

Fig. 3 shows at the solid –fluid inter surface of the fluid , the fluid micro-rotation (angular velocity of fluid in fluid flow region) field increases asymptotically with the increase in magnetic parameter M. The fluid angular velocity decreases sharply in between $0 < \eta < 2.5$ and when $2.5 < \eta$, it decreases slowly and almost becomes constant. For M=0 and 0.1, micro rotation profiles have points of inflexion in the interval {2,3]. This shows the micro-rotation boundary layer thickness increases with the increase in the magnetic parameter.

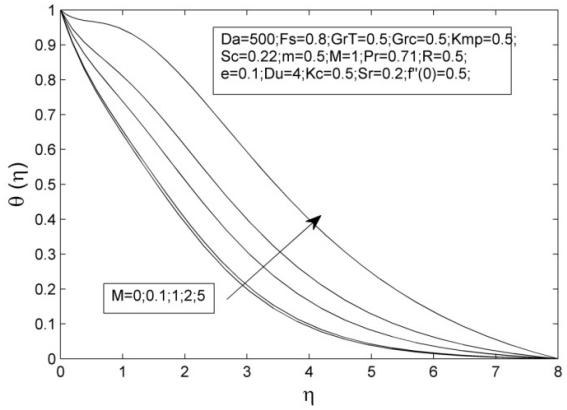

Fig. 4. Variation in the value of temperature with M, the Magnetic parameter

Fig. 4 shows the temperature field increases asymptotically with the increase in magnetic parameter M. The temperature decreases sharply when $0 < \eta < 4$ and when $4 < \eta$, it decreases slowly and almost becomes constant. This shows thermal boundary layer thickness increases with the increase in the magnetic parameter M.

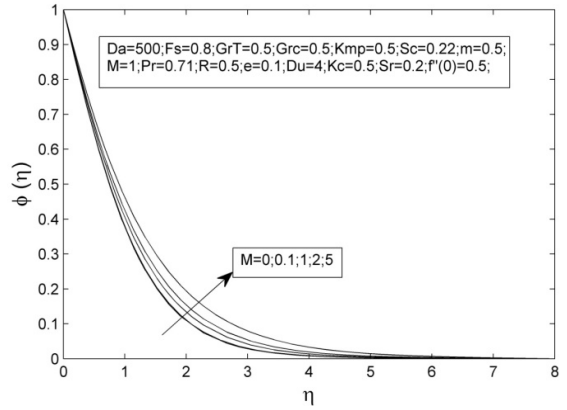

Fig. 5. Variation in the value of concentration with M , the Magnetic parameter

Fig. 5 shows the concentration field increases asymptotically with the increase in magnetic parameter M. The concentration decreases sharply when $0 < \eta < 2.5$ and when $2.5 < \eta$, it decreases slowly and almost becomes constant. This shows concentration boundary layer thickness increases with the increase in the magnetic parameter M.

Fig. 6 shows the velocity field increases asymptotically with the increase in Dufour parameter Du. The velocity increases sharply when $0 < \eta < 2.5$ and when $2.5 < \eta$, it increases slowly and almost becomes constant. This shows velocity boundary layer thickness increases with the increase in the Dufour parameter Du.

Fig. 7 shows at the solid –fluid inter surface of the fluid, the fluid micro-rotation (angular velocity of fluid in fluid flow region) field decreases asymptotically with the increase in Dufour parameter Du. The fluid angular velocity decreases sharply in between $0 < \eta < 2.5$ and when $2.5 < \eta$, it increases slowly and almost becomes constant. For $0 < \eta < 2.5$ micro rotation profiles decrease with the increase in Dufour

parameter Du and for $2.5 < \eta$ micro rotation profiles increase very slowly with the increase in Dufour parameter Du. This shows the micro-rotation boundary layer thickness decreases with the increase in the Dufour parameter Du.

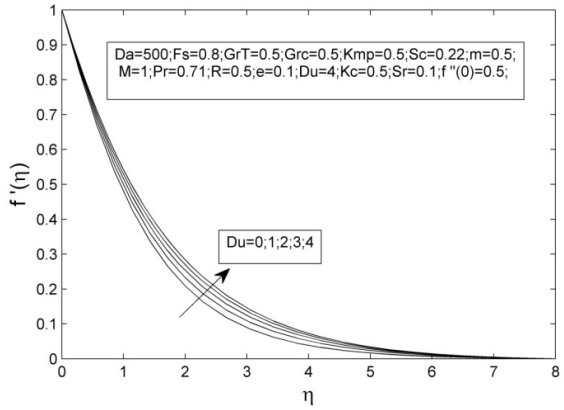

Fig. 6. Variation in the value of fluid velocity with Du, the Dufour parameter

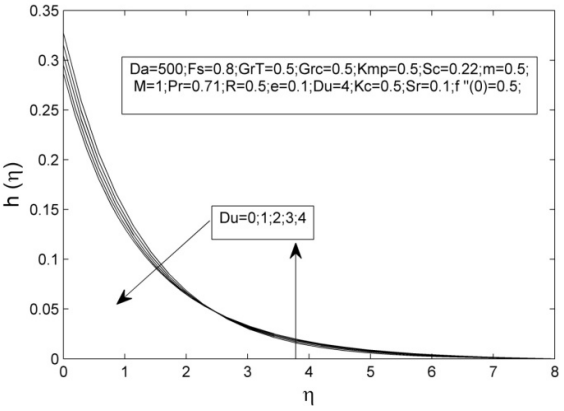

Fig. 7. Variation in the value of angular velocity with Du , the Dufour parameter

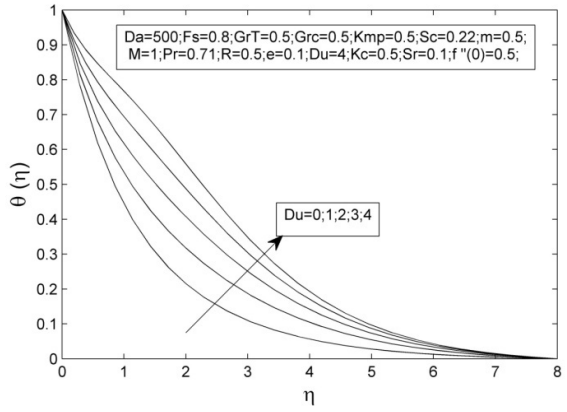

Fig. 8. Variation in the value of temperature with Du, the Dufour parameter

Fig. 8 shows the fluid temperature field increases asymptotically with the increase in the Dufour parameter Du. The temperature increases sharply when $0 < \eta < 4$ and when $4 < \eta$, it increases slowly and almost becomes constant. This shows thermal boundary layer thickness increases with the increase in the Dufour parameter Du.

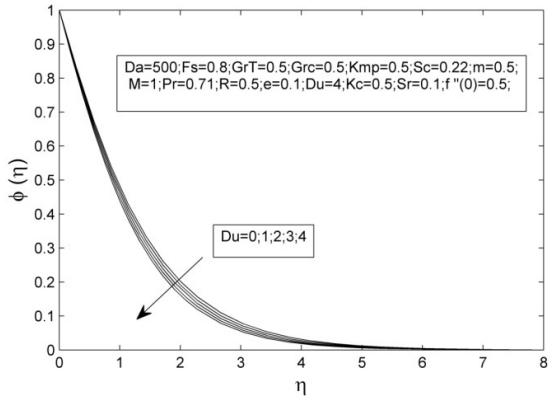

Fig. 9. Variation in the value of concentration with Du , the Dufour parameter

Fig. 9 shows the fluid concentration field decreases asymptotically with the increase in the Dufour parameter Du. The concentration decreases sharply when $0 < \eta < 2.5$ and when $2.5 < \eta$, it decreases slowly and almost becomes constant. This shows concentration boundary layer thickness decreases with the increase in the Dufour parameter Du.

Figs. 10–13, respectively, show the velocity, microrotation, temperature and concentration field for different values of Soret number Sr.

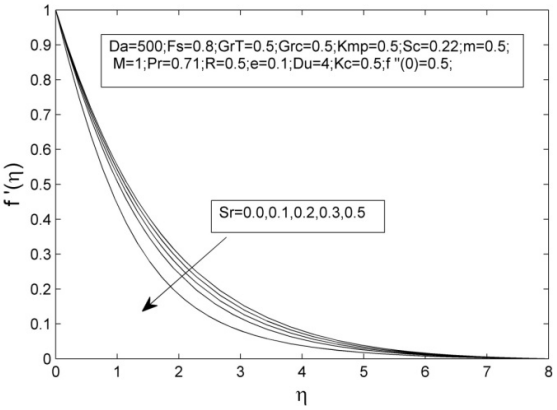

Fig. 10. Variation in the value of fluid velocity with Sr , the Soret parameter

Fig. 10 shows the fluid velocity field decreases asymptotically with the increase in the Soret parameter Sr. The velocity decreases sharply when $0 < \eta < 2.5$ and when $2.5 < \eta$, it decreases slowly and almost becomes constant. This shows velocity boundary layer thickness decreases with the increase in the Soret parameter Sr.

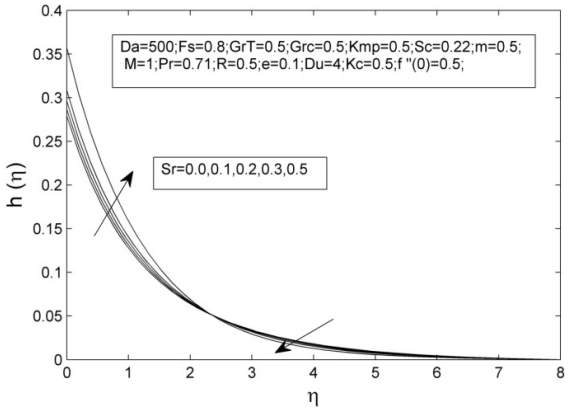

Fig. 11. Variation in the value of angular velocity with Sr, the soret parameter

Fig. 11 shows at the solid –fluid inter surface of the fluid, the fluid micro-rotation (angular velocity of fluid in fluid flow region) field increases asymptotically with the increase Soret parameter Sr. The fluid angular velocity increases sharply in between $0 < \eta < 2.5$ and when $2.5 < \eta$, it decreases slowly and almost becomes constant. For $0 < \eta < 2.5$ micro rotation profiles increase with the increase in Soret parameter Sr and for $2.5 < \eta$ micro rotation profiles decrease very slowly with the increase in Soret parameter Sr. This shows the micro-rotation boundary layer thickness increases with the increase in the Soret parameter Sr.

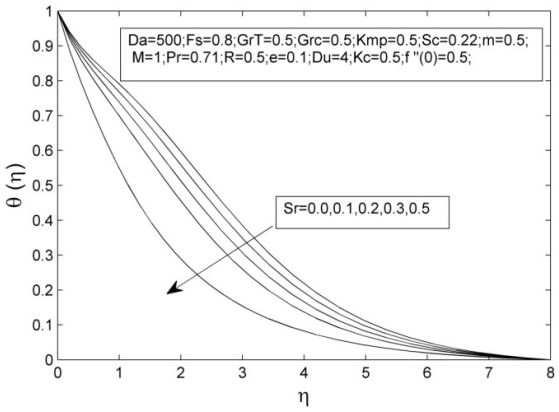

Fig. 12. Variation in the value of temperature with Sr, the soret parameter

Fig. 12 shows the fluid temperature field decreases asymptotically with the increase in the Soret parameter Sr. The temperature decreases sharply when $0 < \eta < 4$ and when $4 < \eta$, it decreases slowly and almost becomes constant. This shows thermal boundary layer thickness decreases with the increase in the Soret parameter Sr.

Fig. 13 shows the fluid concentration field decreases asymptotically with the increase in the Soret parameter Sr. The concentration decreases sharply when $0 < \eta < 2.5$ and when $2.5 < \eta$, it decreases slowly and almost becomes constant. This shows concentration boundary layer thickness decreases with the increase in the Soret parameter Sr.

Figs. 14–17, respectively, show the velocity, microrotation, temperature and concentration field for different values of thermal coefficient ‘e’.

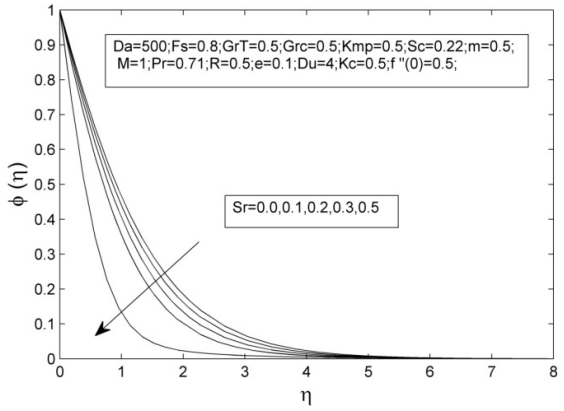

Fig. 13. Variation in concentration with the soret Parameter Sr

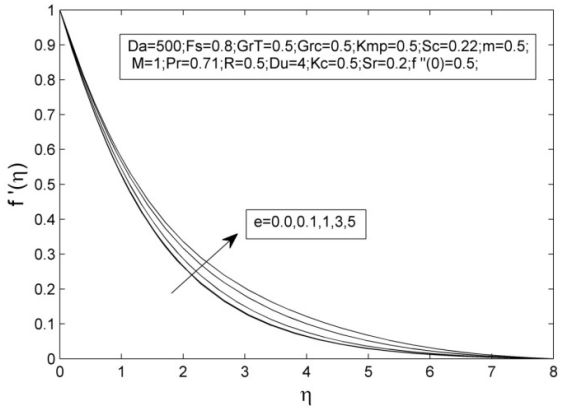

Fig. 14. Variation in the value of fluid velocity with e, the thermal coefficient

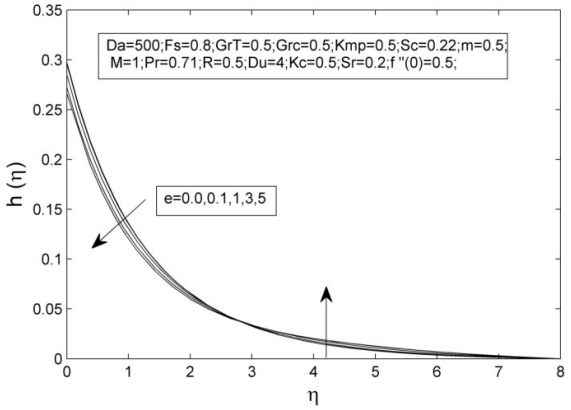

Fig. 15. Variation in the value of angular velocity with e, the thermal coefficient

Fig. 14 shows the fluid velocity field increases asymptotically with the increase in the thermal coefficient 'e'. The velocity increases sharply when $0 < \eta < 2.5$ and when $2.5 < \eta$, it increases slowly and almost becomes constant. This shows velocity boundary layer thickness increases with the increase in the thermal coefficient 'e'.

Fig. 15 shows at the solid –fluid inter surface of the fluid, the fluid micro-rotation (angular velocity of fluid in fluid flow region) field decreases asymptotically with the increase the thermal coefficient 'e' . The fluid angular velocity decreases sharply in between $0 < \eta < 2.5$ and when $2.5 < \eta$, it decreases slowly and almost becomes constant. For $0 < \eta < 2.5$ micro rotation profiles decrease with the increase in the thermal coefficient 'e' and for $2.5 < \eta$ micro rotation profiles increase very slowly with the increase in the thermal coefficient 'e'. This shows the micro-rotation boundary layer thickness decreases with the increase in the thermal coefficient 'e'.

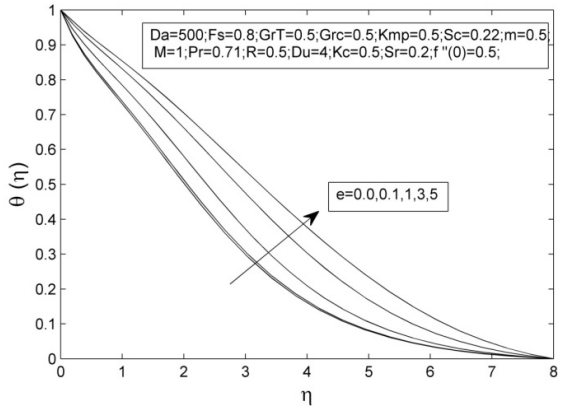

Fig. 16. Variation in the temperature with e, the thermal coefficient

Fig. 16 shows the fluid temperature field increases asymptotically with the increase in the thermal coefficient 'e'. The temperature increases sharply when $0 < \eta < 4$ and when $4 < \eta$, it increases slowly and almost becomes constant. This shows thermal boundary layer thickness increases with the increase in the thermal coefficient 'e'.

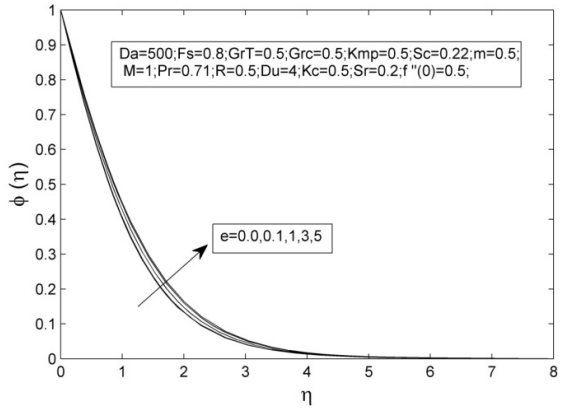

Fig. 17. Variation of concentration with e the thermal coefficient

Fig. 17 shows the fluid concentration field increases asymptotically with the increase in the thermal coefficient 'e'. The concentration increases sharply when $0 < \eta < 2.5$ and when $2.5 < \eta$, it increases slowly and almost becomes constant. This shows concentration boundary layer thickness increases with the increase in the thermal coefficient 'e'.

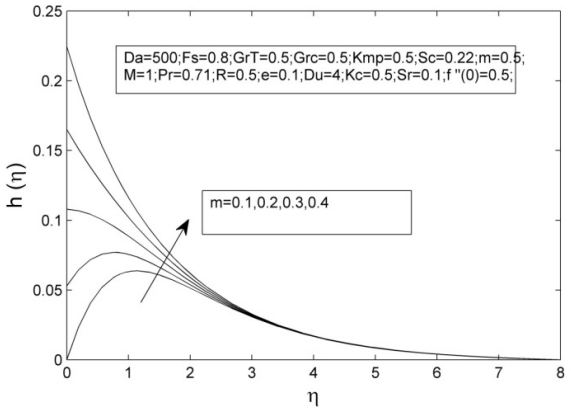

Fig. 18. Variation in the angular velocity with m, the slip parameter

Fig. 18 shows at the solid –fluid inter surface of the fluid , the fluid micro-rotation (angular velocity of fluid in fluid flow region) field increases asymptotically with the increase in the velocity slip 'm'. The fluid angular velocity increases sharply in between $0 < \eta < 2.5$ and when $2.5 < \eta$, it increases slowly and almost becomes constant. For M=0 and 0.1, micro rotation profiles have points of inflexion in the interval {2,3]. This shows the micro-rotation boundary layer thickness increases with the increase in the velocity slip 'm'.

Table 2 shows the effects of the Darcy parameter (Da) on the Skin friction Cf, dimensionless wall couple stress Cr , local Nusselt number Nu , and local Sherwood number Sh. It shows the Skin friction Cf, dimensionless wall couple stress Cr , local Nusselt number Nu and local Sherwood number Sh increases with the increase in the value of Darcy parameter (Da).

Table 2. The values of the skin friction C_f ($f''(0)$), dimensionless surface couple stress C_r ($h'(0)$), Nusselt number Nu ($-\theta'(0)$)and Sherwood number Sh($-\phi'(0)$)for different values of Da and Fs=0.8, GrT=0.6, Grc=0.5, Kmp=0.5, Sc=0.22,M=1, Pr=0.71, R=0.5, e=0.1, Du=4, Kc=0.5, Sr=0.1, f ''(0)=0.5, m=0.5

Da	$f''(0)$	$h'(0)$	$-\theta'(0)$	$-\phi'(0)$
100	-0.5232968998	-0.2130987767	0.4148029270	0.6842387169
300	-0.5203648452	-0.2114961126	0.4155003921	0.6844328942
500	-0.5197776341	-0.2111750671	0.4156400406	0.6844717840

Table 3 shows the effects of the Forchheimer parameter(Fs) on the Skin friction Cf, dimensionless wall couple stress Cr , local Nusselt number Nu and local Sherwood number Sh. It shows the Skin friction Cf, dimensionless wall couple stress Cr, local Nusselt number Nu and local Sherwood number Sh increase with the increase in the value of Forchheimer parameter(Fs).

Table 3. The values of the Skin friction C_f ($f''(0)$), dimensionless surface couple stress C_r ($h'(0)$), local Nusselt number Nu ($-\theta'(0)$)and local Sherwood number Sh($-\phi'(0)$)for different values of Fs and Da=500, Fs=0.8, GrT=0.5, Grc=0.5, Kmp=0.5, Sc=0.22, M=1, Pr=0.71, R=0.5, e=0.1, Du=4, Kc=0.5, Sr=0.1, f ''(0)=0.5, m=0.5

Fs	$f''(0)$	$h'(0)$	$-\theta'(0)$	$-\phi'(0)$
0.4	-0.6923363518	-0.3067500491	0.3800429068	0.6741087526
0.6	-0.6343386592	-0.2738148989	0.3890995886	0.6771447600
0.8	-0.5728824078	-0.2387131577	0.3987757166	0.6803955008

Table 4 shows the effects of the Thermal Grashoff parameter (GrT) on the Skin friction Cf, dimensionless wall couple stress Cr, local Nusselt number Nu ,and local Sherwood number Sh. It shows the Skin friction Cf, dimensionless wall couple stress Cr, local Nusselt number Nu and local Sherwood number Sh increase with the increase in the value of Grashof temperature parameter.

Table 4. The values of the Skin friction Cf, ($f''(0)$),dimensionless wall couple stress Cr , ($h'(0)$),local Nusselt number Nu , ($-\theta'(0)$)and local Sherwood number Sh,($-\phi'(0)$)for different values of GrT and Da=500;Fs=0.8;GrT=0.5;Grc=0.5;Kmp=0.5;Sc=0.22;M=1;Pr=0.71;R=0.5;e=0.1;Du=4;Kc=0.5;Sr=0.1; f ''(0)=0.5;m=0.5;

GrT	$f''(0)$	$h'(0)$	$-\theta'(0)$	$-\phi'(0)$
0.4	-0.7419638023	-0.3220532467	0.3319502829	0.666202065
0.6	-0.6273918455	-0.2663504570	0.3797860892	0.6760412478
0.8	-0.5197776341	-0.2111750671	0.4156400406	0.6844717840

Table 5. The values of the Skin friction Cf, ($f''(0)$),dimensionless wall couple stress Cr , ($h'(0)$),local Nusselt number Nu , ($-\theta'(0)$)and local Sherwood number Sh,($-\phi'(0)$)for different values of Grc and Da=500;Fs=0.8;GrT=0.5;Grc=0.5; Kmp=0.5;Sc=0.22; M=1; Pr=0.71; R=0.5;e=0.1;Du=4;Kc=0.5;Sr=0.1; f ''(0)=0.5;m=0.5;

Grc	$f''(0)$	$h'(0)$	$-\theta'(0)$	$-\phi'(0)$
0.4	-0.6891462664	-0.3027219793	0.3752254971	0.6732310281
0.6	-0.6114477561	-0.2601329838	0.3911533661	0.6780545407
0.8	-0.5344995269	-0.2172142340	0.4061880046	0.6826918568

Table 5 shows the effects of the concentration Grashof parameter (Grc) on the Skin friction Cf, dimensionless wall couple stress Cr, local Nusselt number Nu and local Sherwood number Sh. It shows the Skin friction Cf, dimensionless wall couple stress Cr, local Nusselt number Nu and local Sherwood number Sh increase with the increase in the value of Grashof concentration parameter.

Table 6 shows the effects of the micropolar parameter, K_{mp} on the Skin friction Cf, dimensionless wall couple stress Cr, local Nusselt number Nu and local Sherwood number Sh. It shows the Skin friction Cf, dimensionless wall couple stress Cr, local Nusselt number Nu and local Sherwood number Sh increases with the increase in the value of micropolar parameter.

Table 6. The values of the Skin friction Cf, ($f''(0)$), dimensionless wall couple stress Cr, ($h'(0)$), local Nusselt number Nu, ($-\theta'(0)$) and local Sherwood number Sh, ($-\phi'(0)$) for different values of Kmp and Da=500;Fs=0.8;GrT=0.6;Grc=0.5;Kmp=0.5;Sc=0.22; M=1;Pr=0.71;R=0.5;e=0.1;Du=4;Kc=0.5;Sr=0.1;f ''(0)=0.5;m=0.5;

Kmp	$f''(0)$	$h'(0)$	$-\theta'(0)$	$-\phi'(0)$
0.4	-0.5238358848	-0.2227831673	0.4137682343	0.6840377088
0.6	-0.5156431164	-0.2009795469	0.4174565801	0.6848951515
0.8	-0.5073869212	-0.1837565643	0.4209411691	0.6857081329

Table 7. The values of the Skin friction Cf, ($f''(0)$),dimensionless wall couple stress Cr , ($h'(0)$), local Nusselt number Nu , ($-\theta'(0)$)and local Sherwood number Sh, ($-\phi'(0)$) for different values of Pr and Da=500;Fs=0.8;GrT=0.5;Gec=0.5;Kmp=0.5;Sc=0.22; M=1;m=0.5;R=0.5;e=0.1;Du=4;Kc=0.5;Sr=0.1;f ''(0)=0.5;

Pr	$f''(0)$	$h'(0)$	$-\theta'(0)$	$-\phi'(0)$
1	-0.5877606189	-0.2441906200	0.4890258990	0.6995598113
2	-0.6407913311	-0.2648382955	0.8040876448	0.8002199228
3	-0.7216655338	-0.2978096753	1.1908847741	1.0429179103

Table 7 shows the effects of the Prandtl parameter on the Skin friction Cf, dimensionless wall couple stress Cr, local Nusselt number Nu and local Sherwood number Sh. It shows the Skin friction Cf, dimensionless wall couple stress Cr decrease, local Nusselt number Nu and local Sherwood number Sh increase with the increase in the value of Prandtl parameter.

Table 8. The values of the Skin friction Cf, ($f''(0)$),dimensionless wall couple stress Cr , ($h'(0)$),local Nusselt number Nu , ($-\theta'(0)$)and local Sherwood number Sh,($-\phi'(0)$)for different values of R and Da=500;Fs=0.8;GrT=0.5;Grc=0.5;Kmp=0.5;Sc=0.22; M=1;Pr=0.71;R=0.5;e=0.1;Du=4;Kc=0.5;Sr=0.1;f ''(0)=0.5;m=0.5;

R	$f''(0)$	$h'(0)$	$-\theta'(0)$	$-\phi'(0)$
0.2	-0.5815547952	-0.2418564517	0.4495261450	0.6910481957
0.4	-0.5754249947	-0.2396276727	0.4135433236	0.6833552017
0.6	-0.5706029556	-0.2378983543	0.3856487998	0.6778604185

Table 8 shows the effects of the Radiation parameter on the Skin friction Cf, dimensionless wall couple stress Cr, local Nusselt number Nu and local Sherwood number Sh. It shows the Skin friction Cf, dimensionless wall couple stress Cr increase, local Nusselt number, Nu and local Sherwood number, Sh decrease with the increase in the value of Radiation parameter.

Table 9 shows the effects of the Schmidth parameter on the Skin friction Cf, dimensionless wall couple stress Cr, local Nusselt number Nu and local Sherwood number Sh. It shows the Skin friction Cf, first decreases and then increases, dimensionless wall couple stress Cr increases, local Nusselt number, Nu decreases and local Sherwood number, Sh increases with the increase in the value of Schmidth parameter.

Table 9. The values of the Skin friction Cf, ($f''(0)$),dimensionless wall couple stress Cr , ($h'(0)$), local Nusselt number Nu , ($-\theta'(0)$)and local Sherwood number Sh, ($-\phi'(0)$) for different values of Sc and Da=500;Fs=0.8;GrT=0.5;Grc=0.5;Kmp=0.5;Sc=0.22; M=1;Pr=0.71.0;R=0.5;e=0.1;Du=4;Kc=0.5;Sr=0.1;f ''(0)=0.5;m=0.5

Sc	$f''(0)$	$h'(0)$	$-\theta'(0)$	$-\phi'(0)$
0.2	-0.5721485289	-0.2385879159	0.4294688888	0.6536501214
0.4	-0.5751218924	-0.2384920298	0.1543024516	0.8757812593
0.6	-0.5730513358	-0.2367478821	-0.0840118311	1.0403330825

Table 10. The values of the Skin friction Cf, ($f''(0)$),dimensionless wall couple stress Cr , ($h'(0)$),local Nusselt number Nu , ($-\theta'(0)$)and local Sherwood number Sh, ($-\phi'(0)$)for different values of Kc and Da=500;Fs=0.8;GrT=0.5;Grc=0.5;Kmp=0.5;Sc=0.22; M=1;Pr=0.71;R=0.5;e=0.1;Du=4;Kc=0.5;Sr=0.1;f ''(0)=0.5;m=0.5

Kc	$f''(0)$	$h'(0)$	$-\theta'(0)$	$-\phi'(0)$
0.2	-0.5717526148	-0.2384718973	0.4621701275	0.6279053339
0.4	-0.5725224770	-0.2386371389	0.4195698983	0.6632316926
0.6	-0.5732270304	-0.2387851687	0.3782987599	0.6972477499

Table 10 shows the effects of the Chemical reaction parameter on the Skin friction Cf, dimensionless wall couple stress Cr , local Nusselt number Nu ,and local Sherwood number Sh. It shows the Skin friction Cf, dimensionless wall couple stress Cr, local Nusselt number Nu decrease and local Sherwood number Sh increases with the increase in the value of chemical reaction parameter.

5 Conclusion

In the above work , following problem is studied: the thermo-diffusion and Diffusion-thermo effects on MHD micropolar fluid flow over a linearly stretching sheet, through a non -Darcy porous medium, where stretching velocity of the sheet varies linearly with distance from the origin, and, temperature and concentration vary non linearly in the boundary layer region. From the work following results are obtained.

With the increase in the value of Magnetic parameter 'M', velocity boundary layer thickness decreases, microrotation boundary layer thickness, thermal boundary layer thickness, concentration boundary layer thickness increase.

With the increase in the value of Dufour number 'Du', velocity boundary layer thickness and thermal boundary layer thickness increase while, microrotation boundary layer thickness and concentration boundary layer thickness decrease.

With the increase in the value of Soret number 'Sr', velocity boundary layer thickness and concentration boundary layer thickness decrease while, microrotation boundary layer thickness and thermal boundary layer thickness increase.

With the increase in the value of thermal coefficient 'e', velocity boundary layer thickness, thermal boundary layer thickness and concentration boundary layer thickness increase while, microrotation boundary layer thickness decrease.

With the increase in the value of slip parameter 'm', microrotation boundary layer thickness increases.

The Skin friction C_f dimensionless wall couple stress Cr, local Nusselt number Nu, and local Sherwood number Sh, increase with the increase in the value of Darcy, Forchheimer, Grashoff temperature, Grashoff concentration and micropolar parameters .

As the value of Prandtl parameter increases the Skin friction C_f dimensionless wall couple stress Cr, decrease, and local Nusselt number Nu, and local Sherwood number Sh, increase.

As the value of Radiation parameter increases the Skin friction Cf, dimensionless wall couple stress Cr increase, and local Nusselt number Nu, and local Sherwood number Sh, decrease.

As the value of Schmidth parameter increases the Skin friction C_f first decreases and then increases, dimensionless wall couple stress Cr increases, local Nusselt number Nu decreases and local Sherwood number Sh, increases.

As the value of Chemical reaction parameter increases the Skin friction Cf, dimensionless wall couple stress Cr and local Nusselt number Nu decrease and local Sherwood number Sh, increases.

Competing Interests

Authors have declared that no competing interests exist.

References

[1] Eringen AC. Theory of micropolar fluids. J. Math. Mech. 1960;6:1–18.

[2] Sakiadis BC. Boundary layer behavior on continuous solid surfaces: II. The boundary layer on continuous flat surface. AIChE J. 1961;7:221–225.

[3] Crane LJ. Flow past a stretching plane. Z. Angew. Math. Phys. 1970;21:645–647.

[4] Nield DA, Bejan AA. Convection in porous media. 2nd ed. Springer, New York; 1999.

[5] Lukaszewicz G. Micropolar fluids: Theory and applications, Birkh a¨ user, Boston; 1999.

[6] Srinivasacharya D, Mendu Upendar. Effect of double stratification on MHD free convection in a micropolar fluid. Journal of the Egyptian Mathematical Society. 2013;21:370–378.

[7] Ashwin Ramachandran, Bijaylakshmi Saikia, Krishnendu Sinha, Rama Govindarajan. Effect of Prandtl number on the linear stability of compressible Couette flow. International Journal of Heat and Fluid Flow. 2016;1–9 , Effect of www.elsevier.com/locate/ijheatfluidflow

[8] Asma Khalid, Ilyas Khan, Arshad Khan, and Sharidan Shafie, Conjugate transfer of heat and mass in unsteady flow of a micropolar fluid with wall couple stress, AIP ADVANCES 5. 127125 2015. Available:http://dx.doi.org/10.1063/1.4938551

[9] Sohail Nadeem, Sadaf Masood, Rashid Mehmood, Muhammad Adil Sadiq. Optimal and numerical solutions for an MHD micropolar nanofluid between rotating horizontal parallel plates. PLOS ONE | DOI:10.1371/journal.pone.0124016 June 5, 2015.

[10] Kalidas Das. Slip effects on heat and mass transfer in MHD micropolar fluid flow over an inclined plate with thermal radiation and chemical reaction. Int. J. Numer. Meth. Fluids. 2012;**70**:96–113. DOI: 10.1002/fld.2683

[11] Adhikari A, Maiti AK. MHD micropolar fluid flow towards a vertical surface in presence of heat. Journal of IMVI. 2014;4:1-25.
DOI: 11.7251/JIMVI140101A.

[12] Habibi Matin M, Dehsara M, Abbassi A. Mixed convection MHD flow of nanofluid over a non-linear stretching sheet with effects of viscous dissipation and variable magnetic field ;ISSN 1392 - 1207. MECHANIKA. 2012;18(4):415-423.
Available:http:// dx.doi.org/ 10.5755/ j01.mech.18.4.2334

[13] Chaudhary RC, Abhay Kumar Jha. Effect of chemical reaction on MHD micropolar fluid flow past a vertical plate in slip-flow regime. Appl. Math. Mech. Engl. Ed. 2008, 29(9):1179–1194.
DOI:10.1007/s10483-008-0907-x

[14] Kashif Ali, Muhammad Farooq Iqbal, Zubair Akbar, Muhammad Ashraf. Numerical simulation of unsteady water-based nanofluid flow and heat transfer between two orthogonally moving porous coaxial disks. Journal of Theoretical and Applied Mechanics. 2014;52(4):1033-1046. Warsaw.

[15] Syed Tauseef Mohyud-Din, Saeed Ullah Jan, Umar Khan, Naveed Ahmed. MHD flow of radiative micropolar nanofluid in a porous channel: Optimal and numerical solutions. Neural Comput & Applic.
DOI:10.1007/s00521-016-2493-3.

[16] El-Dabe NT, Ghaly AY, Rizkallah RR., Ewis KM, Al-Bareda AS. Numerical solution of mhd flow of micropolar fluid with heat and mass transfer towards a stagnation point on a vertical plate. American Journal of Computational Mathematics. 2015;**5:**158-174.
Available:http://dx.doi.org/10.4236/ajcm.2015.52013

[17] Srinivas Maripala and Kishan Naikoti. MHD effects on micropolar nanofluid flow over a radiative stretching surface with thermal conductivity. Advances in Applied Science Research. 2016;7(3):73-82. ISSN: 0976-8610.

[18] Ali J. Chamkha RA. Mohamed, Sameh E. Ahmed. Unsteady MHD natural convection from a heated vertical porous plate in a micropolar fluid with Joule heating, chemical reaction and radiation effects. Meccanica.
DOI 10.1007/s11012-010-9321-0

[19] Sandeep N, Sulochana C, Sugunamma V, Raju CSK, Jayachandra Babu M. Unsteady boundary layer flow of thermophoretic MHD nanofluid past a stretching sheet with space and time dependent internal heat source/sink. Appl. Appl. Math. ISSN: 1932-9466. 2015;10(1):312-327.

[20] Khedr MEM, Chamkha AJ, Bayomi M. MHD Flow of a micropolar fluid past a stretched permeable surface with heat generation or absorption. Nonlinear Analysis: Modelling and Control. 2009;14(1): 27–40.

[21] Sandeep N, Sulochana C. Dual solutions for unsteady mixed convection flow of MHD micropolar fluid over a stretching/shrinking sheet with non-uniform heat source/sink. Engineering Science and Technology, an International Journal. 2015;18:738e745.

[22] Satya Narayana PV, Venkateswarlu B, Venkataramana S. Effects of Hall current and radiation absorption on MHD micropolar fluid in a rotating system. Ain Shams Engineering Journal. 2013;4: 843–854.

[23] Kelson NA, Desseaux A. Effects of surface conditions on flow of a micropolar fluid driven by aporous stretching sheet. International Journal of Engineering Science. 2001;39:1881-1897. Available:www.elsevier.com/locatwe/ijen.gsci

[24] Pal D, Chatterjee S. Effects of radiation on Darcy-Forchheimer convective flow over a stretching sheet in a micropolar fluid with non- uniform heat source/sink. Journal of Applied Fluid Mechanics. 2015;8(2):207-212.
Available: www.jafmonline.net, ISSN 1735-3572, EISSN 1735-3645

Peer-review history:
The peer review history for this paper can be accessed here (Please copy paste the total link in your browser address bar)
http://sciencedomain.org/review-history/21217